Comparing firn temperature profile retrieval based on the firn densification model and microwave data over the Antarctica

Xiaofeng Wang[1,2], Lu An[1,2], Peter L. Langen[3], Rongxing Li[1,2]

[1]Center for Spatial Information Science and Sustainable Development, Tongji University, 1239 Siping Road, Shanghai, China
[2]College of Surveying and Geo-Informatics, Tongji University, 1239 Siping Road, Shanghai, China
[3]Department of Environmental Science, iClimate, Aarhus University, Roskilde, Denmark

Keywords: firn temperature profiles, brightness temperature, firn densification model, evaluation, Antarctic

Abstract

The firn temperature is a crucial parameter for understanding firn densification processes of the Antarctic Ice Sheet (AIS). Simulations with firn densification models (FDM) can be conceptualized as a function that relies on forcing data, comprising temperature and surface mass balance, together with tuning parameters determined based on measured depth-density profiles from different locations. The simulated firn temperature is obtained in the firn densification models by solving the one-dimensional heat conduction equation. Microwave satellite data on brightness temperature at different frequencies can also provide remote sensing monitoring of firn temperature variations across the AIS (i.e., the L-band up to 1500 meters). The firn temperature can be estimated by the microwave emission model and the regression method, but these two methods need more observations of temperature profiles for correction and validation. Therefore, we compiled a dataset with temperature profiles and temperature observations with depth around 10 meters. In this work, two methods were used to simulate/retrieve firn temperature across the Antarctic ice sheet. One method estimated the temperature profiles by solving the one-dimensional heat conduction equation driven by reanalyses and regional climate models, which are used in the simulation of FDMs. The other one established a relationship between the multi-frequency brightness temperature data from microwave remote sensing satellites and the firn temperature.

1. Introduction

With global warming since last century, the extraordinary temperature change events are increasing in the Antarctic ice sheet （AIS） (Wille et al., 2024). The firn temperature was influenced by the surface temperature dynamic change, and it plays an essential role in firn densification models (FDMs) and the stability of the AIS because it can influence the firn densification rate and meltwater within the firn (Dunmire et al., 2024). The firn temperature profiles can be derived by using the thermal model and passive-microwave data (Jun et al., 2002). Most FDMs need a thermal model to simulate the heat-diffusion process to estimate the firn densification rate. Temperature-induced correction from FDMs can reach 40% of all the AIS mass balance results. Firn temperature is also a key indicator of the melt happening.

The firn densification is of great significance for estimating the mass balance of the AIS by satellite altimetry, it will cause surface elevation changes (no mass changes), which need to be deducted from the surface height change estimation of altimetry. FDMs are a reasonable method to deduct firn densification impacts on surface height change due to a lack of long-term observations for firn densification rate. The seasonal cycle of firn temperature below 10 m is totally small (<1 k), so the temperature variations usually happen above 10 m (Cullather et al., 2014). The FDMs need the surface mass balance (SMB) and surface temperature as the forcing inputs to simulate the density and temperature evolution with the depth.

In passive microwave remote sensing research, low-frequency passive microwaves, especially those in the C-band and frequencies below 6.9 GHz, have demonstrated the ability to penetrate more than 10 meters into dry snow layers in AIS field experiments and theoretical simulations (Mätzler, 1987). This capability provides a significant perspective for a deeper understanding of the structure and dynamics of the AIS. In contrast, higher-frequency microwaves are more suited for monitoring temperature changes in shallow firn layers. Further studies have shown that V-polarization brightness temperature (Tb) data have a distinct advantage over H-polarization in monitoring temperature changes within the firn layer, due to its higher signal-to-noise ratio. The seasonal temperature variations within the firn layer mainly occur within the top 10 meters. Several research have proved that the Tb data collected by multi-frequency passive microwave remote sensing can effectively retrieve the internal temperature changes within this layer. The Advanced Microwave Scanning Radiometer (AMSR-E) and its successor, the Advanced Microwave Scanning Radiometer 2 (AMSR2), have Tb products for 6 bands of frequencies, namely C (6.9 GHz), X (10.7 GHz), K-(23.8 GHz), Ku (18.7 GHz), Ka (36.5 GHz), and W (89 GHz). These allow them to retrieve the firn temperature variations above 10 meters.

However, both the FDMs temperature simulation and the inversion of firn layer temperatures using passive microwave remote sensing require as much measured data as possible for calibration. Currently, temperature verification experiments for existing FDMs are limited to very few long-term observational data and verification of the model's lower boundary temperature at 10 meters (T10). T10 served as a reliable indicator of the average annual temperature of AIS. The calibration of internal firn temperature inversion using Tb is also based only on single observation sites or model-simulated temperature data.

Therefore, this study collected a large temperature observation dataset with single-measured temperature profiles, multiple measurements of temperature observations, and a widely distributed T10. Then, we simulated the firn temperature at various depths by the FDMs driven by the SMB and surface temperature, and used the Wide Neural Network (WNN) model to retrieve the firn temperature from the 6 bands (C-, X-, Ku-, K-, Ka-, and W-) Tb data at V polarization from AMSR-E/2. The temperature observation dataset will be used to evaluate the performance of these two methods. It will be

2. Dataset

2.1 Observation

The dataset contains 3 types of temperature observations: 1. 18 single-measured temperature profiles which include 16 observations located along the Zhongshan-Dome A traverse, the other 2 observations in the South Pole and Siple dome; 2. 9 multiple measurements temperature profiles observations which include 6 observations located along the Zhongshan-Dome A traverse, 2 observations located at the Dome C, one located in the South Pole; 3. 1006 temperature T10 observations, as shown in the Fig. 1.

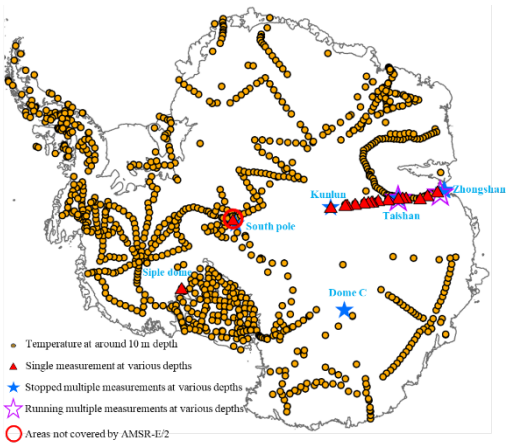

Figure 1. Temperature observations over the AIS (The orange dots are the measured temperature at around 10 m depth; The red triangles represent the single temperature measurements at various depths; The blue solid pentagram is stopped multiple temperature measurements at various depths; The hollow pentagram is the stopped multiple temperature measurements at various depths; The red circle at the South Pole indicates areas not covered by the AMSR-E/2 satellite)

Currently, only the temperature observations at Taishan Station, Dome C Station, 16 observations along the Zhongshan-Dome A traverse and T10 dataset can be simulated and retrieved, because we only have RACMO2.3p2 products that were released before 2020. T10 was evaluated by comparing with the average annual surface temperature.

The evaluation focus on the temperature profiles above 10 m because the temperature variations usually happen above 10 m. From 2016 to 2018, temperature profile observations at Taishan Station were conducted at 1-hour intervals with a depth interval of 0.1 meters. Observations ceased on December 31, 2016, due to battery depletion and resumed on November 13, 2017, following a battery replacement. For the years 2020-2021, the observation frequency at Taishan Station was adjusted to every 4 hours, with a depth interval of 0.5 meters. Between 2006 and 2010, temperature profile observations at Dome C Station were carried out at 1-hour intervals, with a non-uniform depth interval ranging from 0.1 meters to 10 meters. From 2012 to 2016, Dome C Station maintained the same observation frequency and depth intervals; however, data from 2013 to 2015 were excluded from accuracy evaluations due to partial depth data loss. Detailed parameters of the temperature observation instruments are presented in Table 1.

Figures 2a, 2b, 2c, and 2d clearly illustrate the seasonal surface temperature variations of the firn and the process of temperature transfer into the interior. Surface temperature changes have a direct impact on the shallow firn layer above 1 m, with the variation pattern almost identical to that of the surface firn temperature. However, the temperature changes within the deep firn are lagging compared to the surface temperature variations of the firn layer. Figure 2e demonstrates that the internal temperature of the firn decreases with increasing latitude, and in higher latitude regions, the firn temperature remains stable at shallower depths, whereas in lower latitude regions, the depth affected by surface temperature changes is greater.

Table 1 Detailed parameters of the temperature profiles

Stations	Taishan		Dome C	Zhongshan-Dome A traverse
Period	2016-18	2020-21		2018-19
Instrument	DS28EA00	PT1000	PT100	~
Nominal voltage	5 V	5 V		12 V
Working temperature (℃)	- 40~85	-70~85	-100~0	-50 ~ 50
Resolution (℃)	0.0625	0.012	0.02	-
Precision (℃)	-	0.3	0.3	0.2

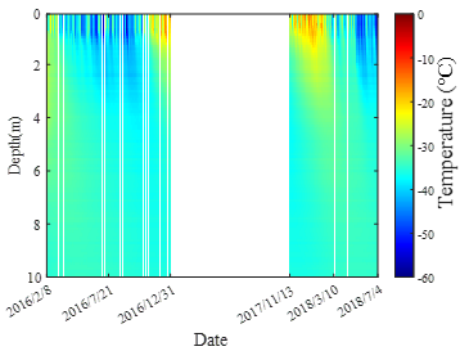

a. The temperature profiles at Taishan station from 2016 to 2018

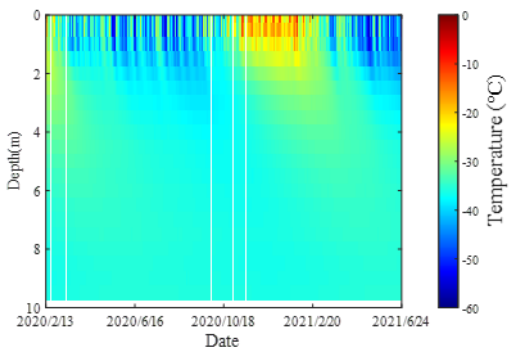

b. The temperature profiles at Taishan station from 2020 to 2021

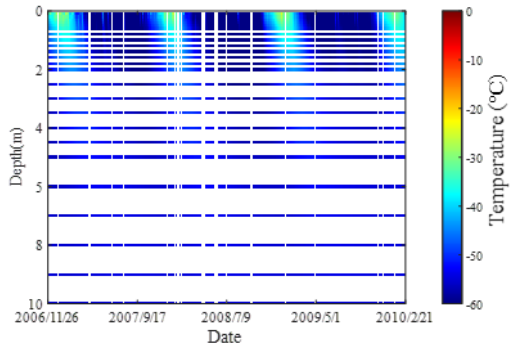

c. The temperature profiles at Dome C station from 2006 to 2010

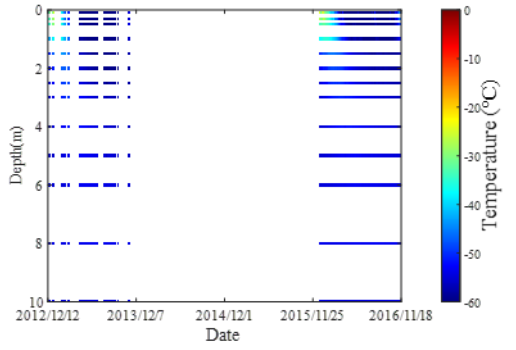

d. The temperature profiles at Dome C station from 2012 to 2016

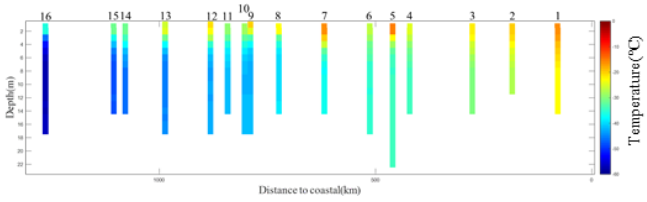

e. The temperature profiles along the Zhongshan-Dome A traverse

Figure 2. The single measurement temperature profiles along the Zhongshan – Dome A traverse and the multiple measurements temperature profiles at Taishan and Dome C stations

2.2 Reanalysis climate model

We selected the RACMO2.3p2 product of SMB and surface temperature as forcing input for the FDMs because our previous work proved that it has the best performance on surface temperature product compared to another 6 climate model products (ERA5, MERRA2, HIRHAM5_ERA-Interim, HIRHAM5_ERA5, MARv3.11, and RACMO2.3p1) over the AIS.

RACMO2.3p2 is a regional climate model developed by the Institute for Marine and Atmospheric Research Utrecht at Utrecht University, which combines the dynamical core of the HIRLAM version6.3.7 and cycle CY33r1 with ECMWF IFS. RACMO2.3p2 forced by ERA5 reanalysis climate model can provide 3-hourly products at 27 km horizontal resolution and vertical resolution of 40 levels, by interactively coupling it to a multilayer snow model that calculates melt, refreezing, percolation, and run-off of meltwater, for snow grain size, background ice albedo, and drifting snow, the model combined with an improved surface albedo scheme, MODIS fields, and a drifting-snow routine. Besides, RACMO2.3p2 updated incorporates upper-air relaxation, a revised topography, tuned parameters in the cloud scheme, and modified snow properties, more detailed information can be found in (van Wessem et al., 2018).

RACMO2.3p2 can provide the SMB and surface temperature products as the forcing input for the FDMs over the AIS, we got the SMB and surface temperature products of RACMO2.3p2 before 2020 from Sanne B. M. Veldhuijsen (Institute for Marine and Atmospheric Research Utrecht, Utrecht University), so only the temperature profiles simulation based on the FDMs before 2020 can be evaluated.

2.3 Brightness data

The radiometer data AMSR-E/2 on NASA's earth observing system Aqua satellite, is available through the National Snow and Ice Data Centre (NSIDC) at the University of Colorado, Boulder . The transit time of AMSR-E/2 satellite are the local times of 01:30 and 13:30. AMSR-E/2 cannot cover the areas around the South Pole, as shown in the Fig.1.

We chose the Level-3 grided products (C- (6.9 GHz), X- (10.7 GHz), Ku- (18.7 GHz), K-(23.8 GHz),Ka- (36.5 GHz), and W- (89 GHz) in both H and V polarizations) of AMSR-E/2 at the resolution of 25 km. Only the C-, X-, Ku-, Ka-, and W- bands at V polarizations was used to retrieve the firn temperature at vary depth because V polarizations product has higher signal-to-noise ratio on firn temperature simulation (Macelloni et al., 2007).

3. Firn temperature simulation

3.1 Temperature Simulation of FDMs

The firn temperature can be derived using the standard one-dimensional heat conduction equation, which adheres to the principle of energy conservation. The heat conduction equation is presented as Eq. (1).

$$\rho c \frac{\partial T}{\partial t} = k\nabla^2 T + \left(\frac{dk}{dz} - \rho c v\right)\frac{\partial T}{\partial z} + f \qquad (1)$$

Where T (unit: K) represents the internal temperature of firn to be solved; c (unit: J kg^{-1} K^{-1}) is the ice heat capacity, which relates to the temperature: c=152.5+7.122T; k (unit: J m^{-1} s^{-1} ℃ $^{-1}$) is thermal conductivity: k = 2×9.828exp(-5.7×10^{-3}T)ρ/(3ρ_I - ρ); v (unit: m a^{-1}) is the vertical velocity: v=A_m/ρ,A_m is the mean accumulation rate to indicate the upper pressure; f is the internal heating, it can be ignored in AIS. ρ (kg/m3) is the firn density at depth z, which is derived from the empirical formula for firn density: $\rho = \rho_i - (\rho_i - \rho_s)\, exp(-Cz)$. The constant C is derived from: C=1.9/Z_t, Z_t is the depth with the density reaches 830 kg m^{-3} according to Ligtenberg and others 2011 (Ligtenberg et al., 2011).

We inputted the SMB to calculate the vertical velocity. In the actual computation process, the surface temperature product from RACMO2.3p2 is employed as the upper boundary condition for the heat conduction equation. The lower boundary condition is set to the annual average surface temperature, with the corresponding depth at 10 meters. The initial condition is established as the surface annual mean temperature. Considering the time required for heat transfer within the firn, the surface temperature from three years prior to the initial observation time is utilized as the input for the upper boundary condition. For setting the density boundary conditions, the surface density is fixed at 300 kg/m^3 as the upper boundary, while the lower boundary condition at the 10 m depth is deduced using an empirical density formula for each site.

3.2 The firn temperature regression model of Tb

In order to accurately retrieve the temperature variations within the firn layer, we assessed the performance of 28 different regression analysis models to find a better model for simulating firn layer temperatures. The models were evaluated using 75% of the data from all microwave bands (C-, X-, Ku-, K-, Ka-, and W-) under V polarization for model training, while the remaining 25% of the data were reserved for model accuracy validation. Evaluation metrics included Mean Absolute Error (MAE), Mean Squared Error (MSE), Root Mean Square Error (RMSE), and Correlation coefficient (R^2). Following this evaluation, WNN is the closest proximity to the observed temperature at 4 depths because it has the least MAE, MSE, RMSE, and R^2, as shown in the Table 2. So, we finally select the WNN regression model to retrieve temperature profiles at 4 depths.

Table 2 The MAE, MSE, RMSE, and R^2 between the retrieved temperature and observed temperature at 1m depth

Model Name	RMSE (℃)	R^2	MAE (℃)	MSE (℃)
Linear Regression	5.68	0.63	4.21	32.21
Interactions Linear Regression	4.27	0.78	2.84	18.27
Robust Linear Regression	6.68	0.51	3.94	44.69
Stepwise Linear Regression	4.32	0.77	2.92	18.70
Fine Tree	4.03	0.80	2.54	16.25
Medium Tree	4.06	0.80	2.61	16.51
Coarse Tree	4.06	0.80	2.69	16.51
Linear SVM	6.44	0.54	3.90	41.43
Quadratic SVM	4.32	0.77	2.85	18.64
Cubic SVM	14.92	0.19	9.04	222.51
Fine Gaussian SVM	4.02	0.80	2.42	16.15
Medium Gaussian SVM	4.20	0.79	2.63	17.62
Coarse Gaussian SVM	4.64	0.74	3.39	21.53
Efficient Linear Least Squares	12.45	0.00	10.99	155.03
Efficient Linear SVM	12.47	0.00	10.94	155.43
Boosted Trees	4.49	0.76	3.12	20.12
Bagged Trees	3.98	0.81	2.47	15.87
Squared Exponential GPR	3.93	0.81	2.48	15.43
Matern 5/2 GPR	3.88	0.82	2.44	15.03
Exponential GPR	3.85	0.82	2.41	14.79
Rational Quadratic GPR	3.86	0.82	2.43	14.93
Narrow Neural Network	3.87	0.82	2.43	14.98
Medium Neural Network	3.88	0.82	2.43	15.08
Wide Neural Network	3.81	0.82	2.33	14.53
Bilayered Neural Network	3.86	0.82	2.41	14.92
Trilayed Neural Network	3.81	0.82	2.34	14.55
SVM Kernel	4.51	0.75	3.12	20.37
Least Squares Regression Kernel	4.55	0.75	3.32	20.73

The WNN regression model is a neural network architecture with a broader structure, featuring more hidden units. It excels in capturing complex relationships in data, particularly in regression tasks, offering automated feature learning and regularization techniques for improved performance. Besides, we applied 5-fold cross-validation to ensure robustness in model evaluation and reduce overfitting.

4. Result

To fairly evaluate the performance of FDMs and the WNN regression model, we calculated the daily temperature by averaging the observed temperature and simulated temperature closest to the passing time of AMSR-E/2 satellite in one day.

We calculated the R^2 between Tb at different frequencies and firn temperature at different depths, as shown in Figure 3. The results indicate that lower-frequency Tb data correlate more closely with firn temperature changes. The frequency band exhibiting the highest correlation is the lower-frequency C band, within which the temperature data at a depth of 5 meters shows the most significant correlation, with an R^2 value of 0.95. This is followed by the temperature data at a depth of 2 meters, which demonstrates a slightly smaller, correlation of 0.85.

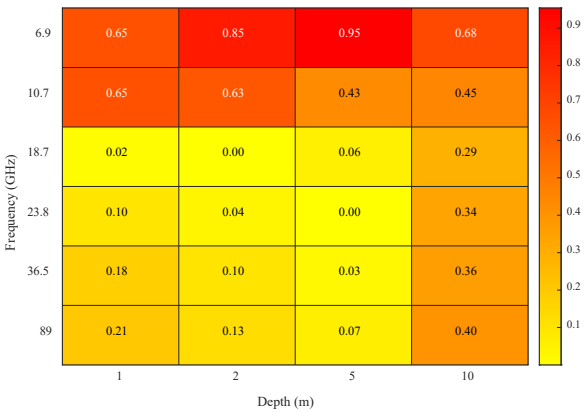

Figure 3. The R^2 between Tb at different frequencies and temperature at different depths

The retrieved firn temperature from Tb and the simulated firn temperature from FDMs on certain depths of 1 m, 2 m, 5 m, and 10 m are displayed in Fig. 4. Both of the retrieved and simulated firn temperature have larger bias, larger RMSE, smaller R^2 with the observed temperature in the shallower depth. The bias, R^2, and RMSE between retrieved/simulated firn temperature and the observed firn temperature decreases as the depth increase.

The performance of the retrieved firn temperature from Tb is better than FDMs at all depths, with smaller bias and RMSE, and higher R^2. Especially above 2 m temperature, the retrieved firn temperature have significant higher R^2 and smaller bias, RMSE. However, the retrieved temperature from Tb has some retrieved temperatures with large deviation at 1m depth. Also, FDMs have some simulated temperatures with large deviation at the 10 m depth.

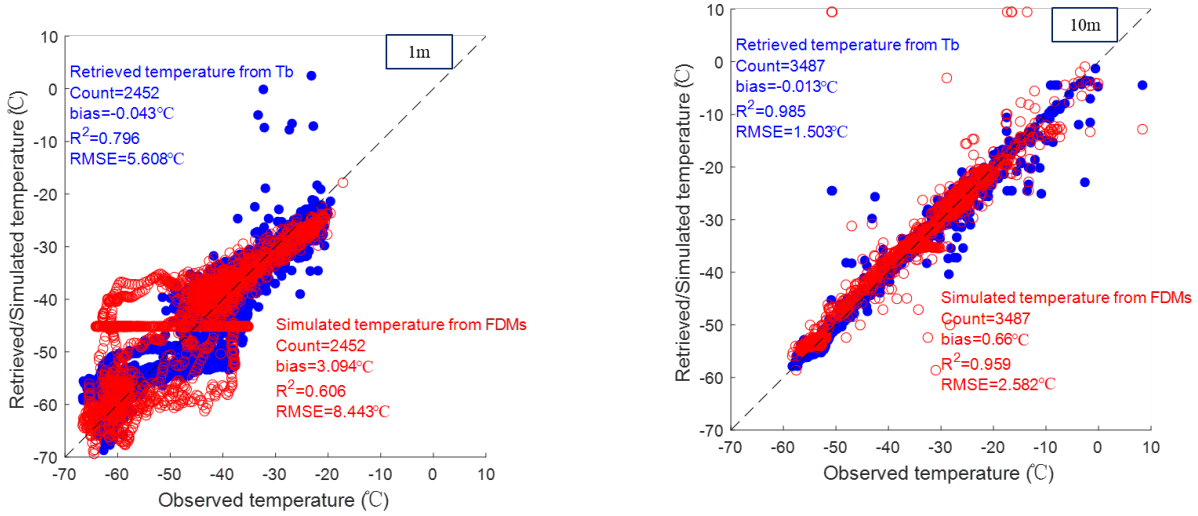

Figure 4. Retrieved/Simulated temperature and observed temperature of firn at 1m, 2m, 5m, and 10m (The blue solid dots is the retrieved firn temperature from the Tb; The red circle is simulated temperature from FDMs)

5. Conclusions

In the context of global warming, accurately predicting firn temperature is crucial for FDMs and AIS mass balance estimation. This study collected a temperature observation dataset with 18 single measured temperature profiles, 9 multiple measurements temperature profiles observations, and 1006 temperature T10 observations over the AIS. Then, we both simulated the firn temperature from FDMs driven by the SMB and surface temperature product of RACMO2.3p2, and retrieved the firn temperature from the WNN model based on the 6 bands (C-, X-, Ku-, K-, Ka-, and W-) Tb at V polarization product of AMSR-E/2 data.

After the evaluation experiments for the retrieved firn temperature from the Tb and the simulated firn temperature, it reveals that the retrieved firn temperature from the Tb data has better performance in predicting firn layer temperature changes at all 4 certain depths compared to the simulated temperature of FDMs. Additionally, the evaluation for the retrieved/simulated temperature at 10 m depth illuminates that we try to use the Tb data to retrieve T10 can improve the accuracy of the lower boundary of FDMs.

This experiment offers a promising solution for the precise retrieval of firn temperature. Based on the post-2020 observations, we aim to further enhance the ability to infer firn temperature change based on Tb data. This will provide valuable support for optimizing temperature parameters in FDMs.

Acknowledgements

This work was supported by the National Key Research and Development Program of China under grants 2021YFB3900105. We thank the support from the Fundamental Research Funds for the Central Universities and the support by the National Key Research and Development Program of China (No. 2017YFA0603100).

References

Cullather, R.I., Nowicki, S.M.J., Zhao, B., Suarez, M.J., 2014. Evaluation of the Surface Representation of the Greenland Ice

Sheet in a General Circulation Model. Journal of Climate 27, 4835–4856. https://doi.org/10.1175/JCLI-D-13-00635.1

Dunmire, D., Wever, N., Banwell, A.F., Lenaerts, J.T.M., 2024. Antarctic-wide ice-shelf firn emulation reveals robust future firn air depletion signal for the Antarctic Peninsula. Commun Earth Environ 5, 1–13. https://doi.org/10.1038/s43247-024-01255-4

Jun, L., Wang, W., Zwally, H.J., 2002. Interannual variations of shallow firn temperature at Greenland summit. Annals of Glaciology 35, 368–370. https://doi.org/10.3189/172756402781816933

Ligtenberg, S.R.M., Helsen, M.M., van den Broeke, M.R., 2011. An improved semi-empirical model for the densification of Antarctic firn. The Cryosphere 5, 809–819. https://doi.org/10.5194/tc-5-809-2011

Macelloni, G., Brogioni, M., Santi, E., 2007. Retrieval from AMSR-E data of the snow temperature profile at Dome-C Antarctica Giovanni Macelloni, in: 2007 IEEE International Geoscience and Remote Sensing Symposium. Presented at the 2007 IEEE International Geoscience and Remote Sensing Symposium, pp. 4233–4236. https://doi.org/10.1109/IGARSS.2007.4423785

Mätzler, C., 1987. Applications of the interaction of microwaves with the natural snow cover. Remote Sensing Reviews. https://doi.org/10.1080/02757258709532086

van Wessem, J.M., van de Berg, W.J., Noël, B.P.Y., van Meijgaard, E., Amory, C., Birnbaum, G., Jakobs, C.L., Krüger, K., Lenaerts, J.T.M., Lhermitte, S., Ligtenberg, S.R.M., Medley, B., Reijmer, C.H., van Tricht, K., Trusel, L.D., van Ulft, L.H., Wouters, B., Wuite, J., van den Broeke, M.R., 2018. Modelling the climate and surface mass balance of polar ice sheets using RACMO2 – Part 2: Antarctica (1979–2016). The Cryosphere 12, 1479–1498. https://doi.org/10.5194/tc-12-1479-2018

Wille, J.D., Alexander, S.P., Amory, C., Baiman, R., Barthélemy, L., Bergstrom, D.M., Berne, A., Binder, H., Blanchet, J., Bozkurt, D., Bracegirdle, T.J., Casado, M., Choi, T., Clem, K.R., Codron, F., Datta, R., Battista, S.D., Favier, V., Francis, D., Fraser, A.D., Fourré, E., Garreaud, R.D., Genthon, C., Gorodetskaya, I.V., González-Herrero, S., Heinrich, V.J., Hubert, G., Joos, H., Kim, S.-J., King, J.C., Kittel, C., Landais, A., Lazzara, M., Leonard, G.H., Lieser, J.L., Maclennan, M., Mikolajczyk, D., Neff, P., Ollivier, I., Picard, G., Pohl, B., Ralph, F.M., Rowe, P., Schlosser, E., Shields, C.A., Smith, I.J., Sprenger, M., Trusel, L., Udy, D., Vance, T., Vignon, É., Walker, C., Wever, N., Zou, X., 2024. The Extraordinary March 2022 East Antarctica “Heat” Wave. Part II: Impacts on the Antarctic Ice Sheet. Journal of Climate 37, 779–799. https://doi.org/10.1175/JCLI-D-23-0176.1